

Top Mass Measurements from Jets and the Tevatron Top-Quark Mass

André H. Hoang^{a*}, Iain W. Stewart^{b†}

^aMax-Planck-Institut für Physik (Werner-Heisenberg-Institut), Föhringer Ring 6, 80805 München, Germany

^bCenter for Theoretical Physics, Massachusetts Institute of Technology, Cambridge, MA 02139

Theoretical issues are discussed for the measurement of the top-mass using jets, including perturbative and non-perturbative effects that relate experimental observables to the Lagrangian mass, and appropriate choices for mass schemes. Full account for these issues is given for $e^+e^- \rightarrow t\bar{t}$ using a factorization theorem for event shapes for massive quarks. Implications for the Tevatron top-mass measurement are discussed. A mass-scheme, the “MSR-mass”, is introduced which allows for a precise description of observables sensitive to scales $R \ll m$, but at the same time does not introduce perturbative matching uncertainties in conversion to the $\overline{\text{MS}}$ mass.

1. Introduction

The top-mass is a key parameter in the standard model. For example, it plays an important role for analyzing electroweak precision constraints, for predicting rare decays like $B \rightarrow X_s \gamma$ and $K_L \rightarrow \pi^0 \nu \bar{\nu}$, as well as for unraveling the Higgs sector in supersymmetric models. The latest measurement from the Tevatron [1], $m_t^{\text{tev}} = 172.6 \pm 0.8(\text{stat}) \pm 1.1(\text{syst})$ GeV, is of very high precision, and brings to mind several theoretical questions. In what mass-scheme is the value quoted? Are measurements of the mass of a colored particle with a precision better than Λ_{QCD} possible using jets, or is this an irreducible uncertainty? How do perturbative and nonperturbative effects modify the relation between the experimental observable and the underlying Lagrangian mass parameter? For the LHC a ~ 1 GeV systematic uncertainty was obtained from preliminary ATLAS studies [2] (where hurdles to go beyond this level include understanding the jet-energy scale to better than 1%). At this level, understanding the answers to the above questions is important.

To achieve a high precision top-mass, measurements exploit kinematic information by consider-

ing leptons + jets, $pp \rightarrow t\bar{t}X \rightarrow (bq\bar{q})(\bar{b}l\bar{\nu})$, or the associated dilepton or all-hadronic channels, and use Monte Carlo (MC) simulations to reconstruct observables sensitive to the top-quark four vector, and hence m_t^2 . One of the most sensitive observables in this reconstruction are the invariant masses $M_a^2 = (\sum_{i \in a} p_i^\mu)^2$ and $M_b^2 = (\sum_{i \in b} p_i^\mu)^2$ of the jets and other decay products produced by the top and antitop respectively. Here the sets a and b depend on the jet-algorithm and cuts. In such analyses it might appear natural to think of the reconstructed top-mass as being associated to the pole-mass m_t^{pole} , since it is designed for sensitivity to the on-shell region $p_t^2 \simeq m_t^2$. However, as we will argue in section 5 below, it is not m_t^{pole} that is being measured by the Tevatron analyses.

The relation of the pole-mass and any other Lagrangian mass-scheme $m_t(R, \mu)$ can be expressed as a perturbative series, $m_t^{\text{pole}} = m_t(R, \mu) + \delta m_t(R, \mu)$ where

$$\delta m_t(R, \mu) = R \sum_{n=1}^{\infty} \sum_{k=0}^n a_{nk} \left[\frac{\alpha_s(\mu)}{4\pi} \right]^n \ln^k \left(\frac{\mu}{R} \right), \quad (1)$$

with R a dimension-1 scale intrinsic to the scheme, and a_{nk} finite numerical coefficients. Theoretically the pole-mass is a poor scheme choice since in QCD its definition is ambiguous by an amount of $\mathcal{O}(\Lambda_{\text{QCD}})$ (in perturbation theory this is referred to as the infrared renormalon

*Talk given at the International Workshop on Top Quark Physics, La Biodola, Isola d’Elba, May 18-24, 2008.

†Talk given at the 2nd Workshop on Theory, Phenomenology and Experiment in Heavy Flavor Physics, Capri, 2008.

problem). Nice mass schemes avoid this problem by a suitable choice for the a_{nk} 's, and are known as short-distance mass schemes. Using observables expressed in terms of short-distance schemes the accuracy that the mass of a colored particle can be measured is not limited by Λ_{QCD} . This fact is important to obtain the $\simeq 40$ MeV uncertainties for current measurements of the b -quark mass [3]. For current top-measurements based on reconstruction there is another important restriction on viable short-distance schemes. In these kinematic-based analyses the top-quark decay is treated with a Breit-Wigner in the MC's, and only "top-resonance mass schemes" with a small $R \sim \Gamma_t$ are compatible with the Breit-Wigner form [4]. This restriction rules out directly measuring the $\overline{\text{MS}}$ mass, which has a much larger $R = m_t$.

To explore these issues in detail it is useful to consider a case with full analytic control, namely jets produced in $e^+e^- \rightarrow t\bar{t}$ with c.m. energy $Q \gg m_t$. Here the jet-invariant masses $M_{t,\bar{t}}$ sum over particles in the top and antitop hemisphere defined with respect to the thrust axis, and are examples of event shape variables for massive quarks. The resonance region $|M_{t,\bar{t}} - m_t| \ll m_t$ is most sensitive to the top-mass. The appropriate factorization theorem was derived in Ref. [4],

$$\begin{aligned} \frac{d^2\sigma}{dM_t^2 dM_{\bar{t}}^2} &= \sigma_0 H_Q(Q, \mu_m) H_m\left(m, \frac{Q}{m}, \mu_m, \mu_\Lambda\right) \\ &\times \int d\ell^+ d\ell^- B_+(\hat{s}_t - \frac{Q\ell^+}{m}, \delta m, \Gamma_t, \mu_\Lambda, \mu_\Gamma) \\ &\times B_-(\hat{s}_{\bar{t}} - \frac{Q\ell^-}{m}, \delta m, \Gamma_t, \mu_\Lambda, \mu_\Gamma) S(\ell^+, \ell^-, \delta\Delta, \bar{\Delta}, \mu_\Lambda), \end{aligned} \quad (2)$$

where $\hat{s}_t \equiv (M_t^2 - m^2)/m$ and $\hat{s}_{\bar{t}} \equiv (M_{\bar{t}}^2 - m^2)/m$. Eq. (2) is valid to all orders in α_s and has power corrections of $\mathcal{O}(m\alpha_s(m)/Q, m^2/Q^2, \Gamma_t/m, \hat{s}_{t,\bar{t}}/m)$. Here H_Q and H_m are perturbative coefficients describing the hard scales Q and m , as well as the summation of large logarithms from $Q \gg m \gg \mu_\Gamma$, where $\mu_\Gamma \sim \Gamma_t + Q\Lambda_{\text{QCD}}/m + \hat{s}_t$. The B_\pm are perturbatively calculable heavy-quark jet functions, which describe the evolution and subsequent decay of the top/antitop quark to jets, and include a resummation of large logs between μ_Γ and the soft scale

$\mu_\Lambda \gtrsim \Lambda_{\text{QCD}} + m\Gamma_t/Q + m\hat{s}/Q$. A complete resummation of large logs at next-to-leading order (NLL) was carried out in Ref. [5], where the reader can find further details. In Eq. (2) m and δm are specified in a top-resonance mass-scheme, of which an example known as the jet-mass is discussed below in section 2. Finally, S is the hemisphere soft-function describing the soft-radiation between jets. S is perturbatively calculable for $\ell^\pm \gg \Lambda_{\text{QCD}}$ and non-perturbative for $\ell^\pm \sim \Lambda_{\text{QCD}}$. The parameter $\bar{\Delta}$ is a gap in the soft function [6], while $\delta\Delta$ indicates that the scheme for this gap is defined so that both perturbative and nonperturbative contributions are included without inducing a leading renormalon ambiguity, as discussed below in section 3.

The result in Eq. (2) relates an experimentally measurable hadronic observable, $d^2\sigma/dM_t^2 dM_{\bar{t}}^2$, to the short distance mass m . As an example, consider the peak position of the invariant mass distribution $M_{t,\bar{t}} = M^{\text{peak}}$. Schematically this relation has the form

$$M^{\text{peak}} = m + \Gamma_t(\alpha_s + \alpha_s^2 + \dots) + \frac{Q\Lambda_{\text{QCD}}}{m}, \quad (3)$$

where the perturbative shifts $\sim \Gamma_t(\alpha_s + \alpha_s^2 + \dots)$ can be calculated from the jet-functions, B_\pm , and the nonperturbative shift $\sim Q\Lambda_{\text{QCD}}/m$ is completely determined by the soft-function S . Having a systematic separation of the perturbative and non-perturbative shifts into B_\pm and S is important for a precision determination of the Lagrangian mass m . In particular the value of the terms in the perturbative series in Eq. (3) are related to the choice of mass-scheme for m , and are modified by different scheme choices. Thus, control over the mass-scheme requires control over these corrections. Note that the non-perturbative shift is always positive for hemisphere masses, and quite sizeable, $\simeq 1\text{--}2$ GeV for typical values of Q . In sections 2 and 3 below we discuss the functions responsible for these perturbative and nonperturbative shifts in more detail. Then in section 4 we quantitatively analyze the relation between M^{peak} and m using Eq. (2). Finally, in section 5 we return to implications for the Tevatron mass, and discuss a very useful mass-scheme for measuring both top and bottom heavy-quark

masses, the MSR-scheme.

2. Heavy-Quark Jet Function

Since $\hat{s} \ll m$ the jet function can be formulated in the heavy-quark limit with HQET,

$$\mathcal{L}_{\text{HQET}} = \bar{h}_v \left(i v \cdot D - \delta m + \frac{i\Gamma_t}{2} \right) h_v. \quad (4)$$

Here $\delta m = m^{\text{pole}} - m$ encodes the mass-scheme choice, and Γ_t is the total width of the top-quark which suffices since our observable is inclusive in the decay products. The heavy-quark jet function is defined as the imaginary part of a h_v propagator connected by a light-like Wilson line [4], $B(\hat{s}, \delta m, \Gamma_t, \mu) = \text{Im}[\mathcal{B}(\hat{s}, \delta m, \Gamma_t, \mu)]$ where

$$\mathcal{B}(\hat{s}, \delta m, \Gamma_t, \mu) = \frac{-i}{m} \int \frac{d^4 x}{4\pi N_c} \langle 0 | T \bar{h}_v(0) W_n(0) W_n^\dagger(x) h_v(x) | 0 \rangle. \quad (5)$$

At tree level in α_s we have a Breit-Wigner, $B = \Gamma_t / [(\pi m)(\hat{s}^2 + \Gamma_t^2)]$. From Eq. (4) the jet function obeys the shift identity $\mathcal{B}(\hat{s}, \delta m, \Gamma_t, \mu) = \mathcal{B}(\hat{s} - 2\delta m + i\Gamma_t, 0, 0, \mu) \equiv \mathcal{B}(\hat{s} - 2\delta m + i\Gamma_t, \mu)$. It also has an RGE $\mu d/d\mu \mathcal{B}(\hat{s}, \mu) = \int d\hat{s}' \gamma_B(\hat{s} - \hat{s}', \mu) \mathcal{B}(\hat{s}', \mu)$ where the anomalous dimension has a plus-function term with the universal cusp anomalous dimension and a δ -function term, $\gamma_B(\hat{s}, \mu) = -2\Gamma_{\text{cusp}}[\alpha_s]/\mu[\mu\theta(\hat{s})/\hat{s}]_+ + \gamma_B[\alpha_s]\delta(\hat{s})$. Summing logarithms from μ_Γ to μ_Λ gives

$$B(\hat{s}, \delta m, \Gamma_t, \mu_\Lambda, \mu_\Gamma) = \int d\hat{s}' U_B(\hat{s} - \hat{s}', \mu_\Lambda, \mu_\Gamma) B(\hat{s}', \delta m, \Gamma_t, \mu_\Gamma), \quad (6)$$

which is the function $B = B_+ = B_-$ appearing in Eq. (2). Eq. (6) sums all logs that can affect the shape of $d^2\sigma/dM_t^2 dm_t^2$ [5]. There is some freedom in combining fixed order results for B at μ_Γ with the RGE in U_B . We define a counting that elevates the importance of fixed order results

LL: 1-loop Γ_{cusp} , tree-level matching; (7)

NLL: 2-loop Γ_{cusp} , 1-loop γ_B and matching;

NNLL: 3-loop Γ_{cusp} , 2-loop γ_B and matching.

One-loop results for B and γ_B were computed in Ref. [5], and two-loop results in Ref. [7]. The three-loop result for Γ_{cusp} is known from Ref. [8],

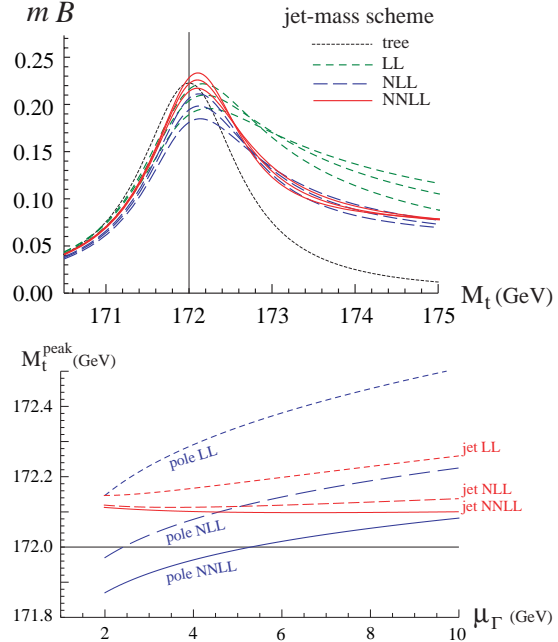


Figure 1. Heavy quark jet-function up to NNLL order (top). Peak positions in the pole and jet-mass schemes (bottom). Plots from [7].

so B is known at NNLL. Results for B in moment space have also been computed [10,9]. A different heavy quark jet function also occurs in the massive quark form factor, whose anomalous dimension shares several coefficients in common with γ_B [9].

In order to implement a short-distance mass-scheme and subtract the infrared contributions related to the pole-mass renormalon we must systematically expand in δm to the same level in α_s that we determine B itself. Writing

$$\delta m = Re^{\gamma_E} \left\{ \frac{\alpha_s(\mu)}{\pi} \delta m_1 + \left[\frac{\alpha_s(\mu)}{\pi} \right]^2 \delta m_2 \right\}, \quad (8)$$

with $R \sim \Gamma_t$, the remaining freedom in specifying the mass-scheme at two-loop order corresponds to defining $\delta m_{1,2}$. The jet-function itself can be used to define a jet-mass scheme, $m = m_J(R, \mu)$ [4]. It is convenient to use the position space jet-function $\tilde{B}(y, \mu)$ so that m_J has a consistent μ -anomalous dimension [7], and we define

$$\delta m_J \equiv \frac{Re^{\gamma_E}}{2} \left. \frac{d \ln \tilde{B}(y, \mu)}{d \ln(iy)} \right|_{iy e^{\gamma_E} = 1/R}. \quad (9)$$

This definition for the jet mass is possible for any value of R , and the anomalous dimension in R can also be consistently derived [11].

In Fig. 1 (top panel) we show results for Eq. (6) using $R = 0.8$ GeV, the jet-mass with reference value $m_J(R, 2.0 \text{ GeV}) = 172$ GeV, $\mu_\Lambda = 1$ GeV, and three curves at each of LL, NLL, and NNLL order corresponding to $\mu_\Gamma = 3.3, 5.0, 7.5$ GeV. Convergence by NNLL is evident. In the bottom panel of Fig. 1 we compare the pole and jet-mass schemes and show that very good convergence for the peak position is achieved in the jet-mass scheme.

3. Hemisphere Soft Function

The hemisphere soft function is defined by a matrix element of Wilson lines

$$S_{\text{hemi}}(\ell^+, \ell^-, \mu) = \frac{1}{N_c} \sum_{X_s} \delta(\ell^+ - k_s^{+a}) \delta(\ell^- - k_s^{-b}) \times \langle 0 | \bar{Y}_{\bar{n}}(0) Y_n(0) | X_s \rangle \langle X_s | Y_n^\dagger(0) \bar{Y}_{\bar{n}}^\dagger(0) | 0 \rangle, \quad (10)$$

where $Y_n^\dagger(0) = P \exp(ig \int_0^\infty ds n \cdot A(ns))$ and $\bar{Y}_{\bar{n}}^\dagger$ is similar but in the $\bar{3}$ representation. Here k_s^{+a} is the sum of all plus-momenta of particles in X_s in hemisphere a , and k_s^{-b} is the sum of all minus-momenta for particles in hemisphere b . Thus the δ -functions in Eq. (10) are a reflection of the prescription for assigning soft-radiation to the invariant masses M_t and $M_{\bar{t}}$. This soft function is universal [4], the same function appears in the factorization theorem for the hemisphere invariant mass distribution as well as the thrust and heavy jet mass distributions of massless jets [12].

$S(\ell^+, \ell^-, \mu)$ has both perturbative and non-perturbative components, and a convenient way to account for this is [6]

$$S(\ell^+, \ell^-, \delta\Delta, \bar{\Delta}, \mu_\Lambda) = \int d\ell'^+ d\ell'^- \quad (11) \\ \times S^{\text{part}}(\ell^+ - \ell'^+, \ell^- - \ell'^-, \delta\Delta, \mu_\Lambda) S^{\text{mod}}(\ell'^+, \ell'^-, \bar{\Delta}).$$

Here S^{part} refers to a partonic computation of Eq. (10) and encodes the proper μ_Λ dependence and large ℓ^\pm behavior into S . S^{mod} is a model for the non-perturbative $\ell^\pm \sim \Lambda_{\text{QCD}}$ region of S . A gap $\theta(\ell'^+ - \bar{\Delta})\theta(\ell'^- - \bar{\Delta})$ is contained

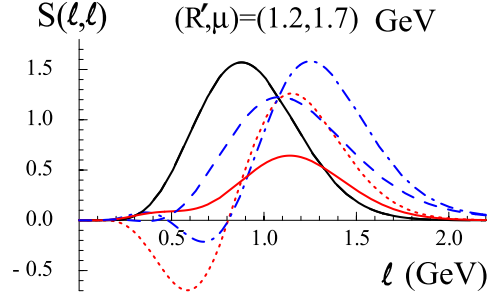


Figure 2. Diagonal hemisphere soft function up to NNLO order in the $\delta\Delta = 0$ scheme and scheme from Eq. (13). Plot from [13].

in S^{mod} where $\bar{\Delta}$ is defined in a scheme specified by $\delta\Delta(R', \mu)$. The partonic soft-function obeys $S^{\text{part}}(\ell^+, \ell^-, \delta\Delta, \mu) = S^{\text{part}}(\ell^+ - \delta\Delta, \ell^- - \delta\Delta, 0, \mu) \equiv S^{\text{part}}(\ell^+ - \delta\Delta, \ell^- - \delta\Delta, \mu)$. To avoid a $\mathcal{O}(\Lambda_{\text{QCD}})$ renormalon (which has nothing to do with the $\mathcal{O}(\Lambda_{\text{QCD}})$ renormalon of quark masses), we must systematically expand in $\delta\Delta$ to the same level in α_s as we expand S^{part} [6]. We write

$$\delta\Delta = R' e^{\gamma_E} \left\{ \frac{\alpha_s(\mu)}{\pi} \delta\Delta_1 + \left[\frac{\alpha_s(\mu)}{\pi} \right]^2 \delta\Delta_2 \right\}. \quad (12)$$

Removing the renormalon with $\delta\Delta$ avoids having to make large changes to S^{mod} each time an additional order in α_s is included in S^{part} . Much like Eq. (9) we can define $\delta\Delta$ with the position space soft function [13], which yields a scheme for $\bar{\Delta}(R, \mu)$ with a consistent RGE in μ and R

$$\delta\Delta = R' e^{\gamma_E} \frac{d \ln \tilde{S}_{\text{part}}(x_1, x_2, \mu)}{d \ln(ix_1)} \Big|_{ie^{\gamma_E} x_{1,2}=1/R'}. \quad (13)$$

Results for $S^{\text{part}}(\ell^+, \ell^-, \delta\Delta, \mu)$ are known at one-loop order [5] and two-loop order [13], and for the thrust soft-function in Refs [14].

In Fig. 2 we compare results for Eq. (11) at LO (black), NLO (blue), and NNLO (red), in the $\delta\Delta = 0$ scheme (dotted & dot-dashed) and in the $\bar{\Delta}$ -scheme (dashed & solid). For S^{mod} we use the 2d-exponential model of Ref. [15] with the addition of the gap $\bar{\Delta}$. The negative dips at small ℓ that are present in the $\delta\Delta = 0$ scheme, are removed in the renormalon free $\bar{\Delta}$ -scheme, and a stable result is obtained for the peak-position of the soft function.

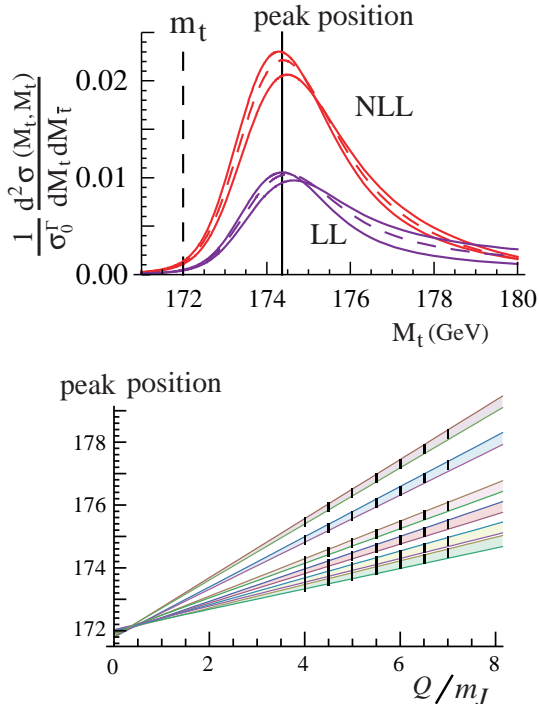


Figure 3. Diagonal invariant mass distribution at LL and NLL order (top). Peak position of the NLL distribution for different soft function models versus Q/m (bottom). Vertical black lines indicate theory uncertainties and the colored bands linear extrapolations to $Q/m \rightarrow 0$. Plots from [5].

4. NLL $e^+e^- \rightarrow t\bar{t}$ Cross-Section

We now proceed to put together all the ingredients in Eq. (2) at NLL order [5] (since the full NNLL results have not yet been published). The cross-section depends on $\mu_Q \sim Q$, $\mu_m \sim m$, μ_Γ , and μ_Λ , and the dependence on these four renormalization scales is reduced from LL to NLL order. The largest variation occurs for μ_Γ and μ_Λ , but is highly correlated. It becomes significantly smaller if we vary fixing $\mu_\Gamma/\mu_\Lambda = Q/m$, which is consistent with the scaling given below Eq. (2). Fig.3 (top panel) shows the invariant mass distribution for $M_t = M_{\bar{t}}$ where the three curves at each order have $\mu_\Gamma = 3.3, 5.0, 7.5$ GeV and the same reference top-mass of 172 GeV was used as in Fig. 1. The $\mathcal{O}(\Lambda_{\text{QCD}})$ renormalons associated to the pole-mass and the partonic soft-function,

both would cause bigger shifts to the location of the invariant mass peak than the difference ($\simeq 0.15$ GeV) between LL and NLL order shown in Fig. 3. Thus using mass and gap schemes that avoid these renormalons was important to obtain perturbative stability. The largest correction to $M_t^{\text{peak}} - m$ is due to the soft radiation, which causes the majority of the difference between the dashed and solid vertical lines of Fig.3 (top panel). The advertised shift, $\propto Q\Lambda_{\text{QCD}}/m$, is demonstrated in Fig. 3 (bottom) where we show that linear dependence on Q occurs for six different models for S^{mod} . For all models the extrapolations to $Q/m \rightarrow 0$ converge to the underlying Lagrangian mass value m . In an e^+e^- environment the correction $M_t^{\text{peak}} - m$ can be determined a) from measurements of S for massless jets that together with perturbative computations determine the shift as in Fig. 3 (top), or b) from measurements at different Q 's with a linear extrapolation that removes the soft-radiation effect as in Fig. 3 (bottom).

5. Implications for the Top Mass in MC programs and the Tevatron Top Mass

The situation at high energy hadron colliders is somewhat different from e^+e^- collisions due to the more complicated initial state and because the jet algorithms needed for the reconstruction of the invariant mass distribution are implemented in terms of MC programs rather than a factorization theorem. Nevertheless, the principles upon which final state interactions in MC's for tops are based, have close analogues with elements in the factorization theorem (2). These analogies make it obvious that the top quark masses contained in MC programs, which are measured at the Tevatron and LHC, are very similar to the jet mass definition we discussed above. Moreover, the Tevatron top mass measurements are statistically dominated by the reconstructed invariant mass distribution in the peak region, which allows more reliable statements to be made about the scheme of the Tevatron top mass.

The final state shower in MC's describes the perturbative aspects of collinear and soft radiation of partons. Starting at transverse scales of

order the momentum transfer of the primary partons the parton shower evolves the system down to the shower cutoff scale R_{sc} which is typically in the 1 GeV range. For the top quark the width $\Gamma_t \approx 1.5$ GeV provides an additional natural shower cutoff for radiation off the top quark. In the factorization theorem (2) the same physics is described by the renormalization group running of the factors H_Q and H_m , the partonic contributions in the soft function and, in particular, the jet functions B_{\pm} . As far as the question of the mass scheme implemented in MC's is concerned, the analogue of the shower cutoff R_{sc} is the modification of the jet functions B_{\pm} due to the residual mass term δm , which subtracts low-energy fluctuations of the jet functions, absorbing them into the mass definition. It is therefore the implementation of the parton shower for the top quark and the size of the shower cutoff R_{sc} which determines the top mass definition used in the MC's.

Another important ingredient of MC's is the description of nonperturbative effects in the hadronization process through models that depend on many parameters. These are fixed from reference processes. For the factorization theorem (2) the analogue of the hadronization models is the soft function which can be determined from event-shapes involving light quark jets. We note that at hadron colliders the treatment of nonperturbative effects is more involved due to the partonic initial state, and does not necessarily lead to a positive shift of the peak position.

For hadron collisions at the Tevatron and the LHC there are additional complications due to for example underlying events, more involved combinatorial background and initial state showers. However, if such effects are modeled correctly in the MC's they do not affect the correspondences mentioned above. We therefore conclude that the top quark mass that is implemented in MC's has the property

$$\delta m_t^{\text{MC}}(R_{sc}) = R_{sc} \left[\frac{\alpha_s(\mu)}{\pi} \right] + \dots \quad (14)$$

with $R_{sc} \sim \Gamma_t \sim 1$ GeV. The exact coefficients in the series on the RHS depend on how the parton shower is implemented and are currently unknown. However, it is reasonable to assume

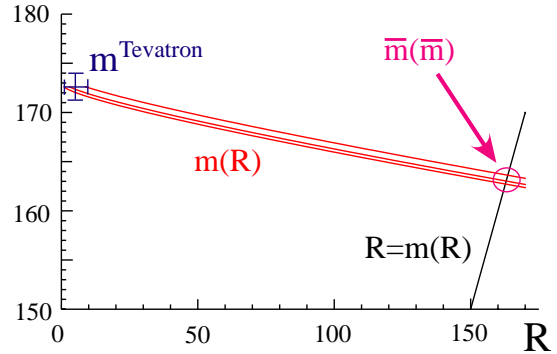


Figure 4. Converting the Tevatron top mass into the $\overline{\text{MS}}$ scheme using the MSR scheme.

that they are of order one. Numerically, the MC masses are therefore quite close to the jet mass scheme defined in (9) for which $R \sim R_{sc}$ or to any other short-distance mass scheme that falls in the category of (1) with $R \sim R_{sc}$.

A good way to illustrate the numerical size of the scheme uncertainty due to the ignorance of the coefficients in (14) is the associated uncertainty in the $\overline{\text{MS}}$ top mass $\overline{m}_t(\overline{m}_t)$. This uncertainty is essential for fits of electroweak precision observables and the resulting indirect Higgs mass bounds. To avoid large logarithms in the perturbative relation of the MC or the jet mass (with $R \sim 1$ GeV) and the $\overline{\text{MS}}$ mass (with $R \sim m_t$), one can use the evolution equation in R from Ref. [11]. Conversions involving the $\overline{\text{MS}}$ mass $\overline{m}_t(\overline{m}_t)$ are particularly simple when the R -evolution is carried out with the MSR-mass scheme $m_t^{\text{MSR}}(R)$, which is a short-distance mass scheme that also falls in the category of (1) and has in addition the property $m_t^{\text{MSR}}(m_t^{\text{MSR}}) = \overline{m}_t(\overline{m}_t)$. The MSR mass definition is obtained from the $\overline{\text{MS}}$ -pole series by a simple replacement rule [11]. We can identify the MSR mass at a low scale R in the 1 GeV range with the mass that is contained in MC programs,

$$m_t^{\text{MC}}(R_{sc}) = m_t^{\text{MSR}}(3_{-2}^{+6} \text{ GeV}). \quad (15)$$

The variation of R between 1 and 9 GeV parameterizes our remaining ignorance.

We now identify $m_t^{\text{MC}}(R_{sc})$ with the Tevatron measurement $m_t^{\text{tev}} = 172.6 \pm 0.8(\text{stat}) \pm 1.1(\text{syst})$ GeV [1]. The result for $\overline{m}_t(\overline{m}_t)$ is il-

lustrated in Fig. 4. The vertical error bars on the Tevatron mass are the experimental uncertainties and the horizontal error bars reflect the current scheme uncertainty due to Eq. (15). The three red lines show the 3-loop R-evolution of the scheme uncertainty with the MSR mass. The intersection of the red lines with the black line that shows the equation $m_t^{\text{MSR}}(R) = R$, gives the $\overline{\text{MS}}$ top mass $\overline{m}_t(\overline{m}_t) = 163.0 \pm 1.3_{-0.3}^{+0.6}$ GeV [11]. Here the first error is the combined experimental one, and the second error is from the scheme uncertainty in the Tevatron mass.

The above correspondence between the shower MC and the factorization theorem is compelling for large p_T events where top quarks are fast. A potential concern is that tops at the Tevatron are produced with predominantly small p_T and are therefore slow. However given that the MC framework applies to this situation, the concept of the top-mass intrinsic to the MC should be independent of whether the MC is applied to energetic tops or to soft tops, and hence the correspondence we have discussed should be applicable for the Tevatron as well. Further study of this is warranted.

This work was supported in part by the Department of Energy Office of Nuclear Science under the grant DE-FG02-94ER40818, and the EU network contract MRTN-CT-2006-035482 (FLAVIANet). IWS was also supported by the DOE OJI program and Sloan Foundation.

REFERENCES

1. T. T. E. Group *et al.* arXiv:0803.1683 [hep-ex].
2. I. Borjanovic *et al.*, Eur. Phys. J. C **39S2**, 63 (2005) [arXiv:hep-ex/0403021].
3. W. M. Yao *et al.* [Particle Data Group], J. Phys. G **33**, 1 (2006).
4. S. Fleming, A. H. Hoang, S. Mantry and I. W. Stewart, Phys. Rev. D **77**, 074010 (2008) [arXiv:hep-ph/0703207].
5. S. Fleming, A. H. Hoang, S. Mantry and I. W. Stewart, Phys. Rev. D **77**, 114003 (2008) [arXiv:0711.2079 [hep-ph]].
6. A. H. Hoang and I. W. Stewart, Phys. Lett. B **660**, 483 (2008) [arXiv:0709.3519 [hep-ph]].
7. A. Jain, I. Scimemi and I. W. Stewart, Phys. Rev. D **77**, 094008 (2008) [arXiv:0801.0743 [hep-ph]].
8. S. Moch, J. A. M. Vermaseren and A. Vogt, Nucl. Phys. B **688**, 101 (2004) [arXiv:hep-ph/0403192].
9. A. Mitov and S. Moch, JHEP **0705**, 001 (2007) [arXiv:hep-ph/0612149].
10. U. Aglietti, L. Di Giustino, G. Ferrera and L. Trentadue, Phys. Lett. B **651**, 275 (2007) [arXiv:hep-ph/0612073]; arXiv:0804.3922 [hep-ph].
11. A. H. Hoang, A. Jain, I. Scimemi and I. W. Stewart, arXiv:0803.4214 [hep-ph].
12. G. P. Korchemsky and G. Sterman, Nucl. Phys. B **555**, 335 (1999) [arXiv:hep-ph/9902341]; C. W. Bauer, C. Lee, A. V. Manohar and M. B. Wise, Phys. Rev. D **70**, 034014 (2004) [arXiv:hep-ph/0309278].
13. A. H. Hoang and S. Kluth, arXiv:0806.3852 [hep-ph].
14. M. D. Schwartz, Phys. Rev. D **77**, 014026 (2008) [arXiv:0709.2709 [hep-ph]]; T. Becher and M. D. Schwartz, JHEP **0807**, 034 (2008) [arXiv:0803.0342 [hep-ph]].
15. G. P. Korchemsky and S. Tafat, JHEP **0010**, 010 (2000) [arXiv:hep-ph/0007005].